

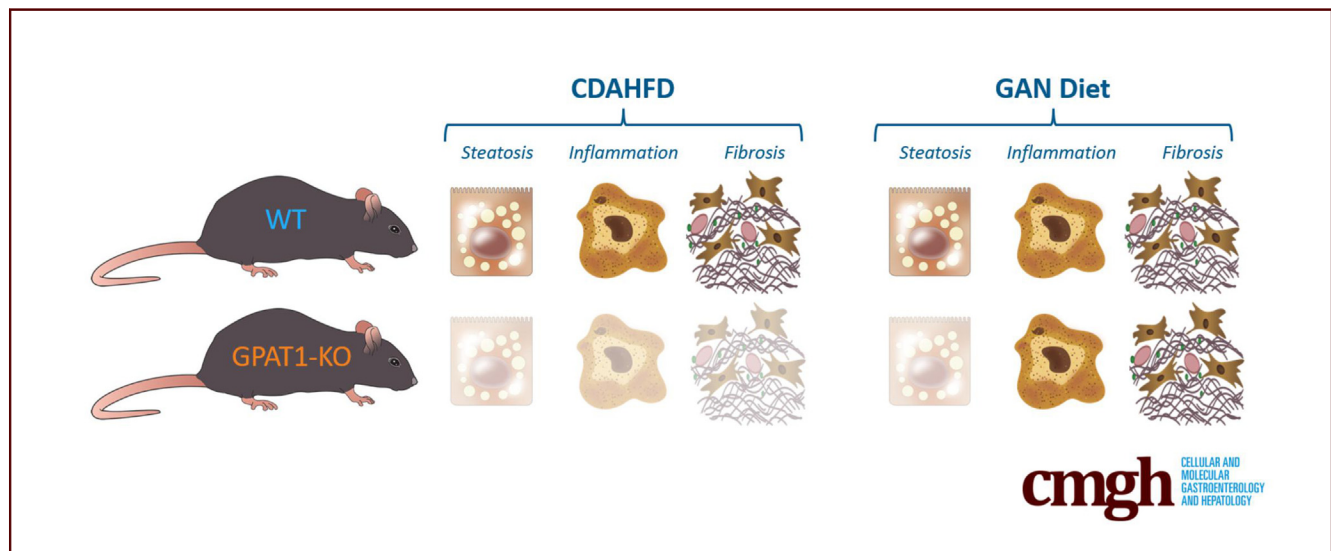
ORIGINAL RESEARCH

GPAT1 Deficiency in Mice Modulates NASH Progression in a Model-Dependent Manner



Kathleen R. Smith,¹ Wenshan Wang,¹ Melissa R. Miller,¹ Magalie Boucher,² Jessica E. Reynold,¹ Natalie A. Daurio,¹ Dongmei Li,¹ Dinesh Hireanallur-Shanthappa,³ Youngwook Ahn,⁴ David A. Beebe,¹ Kenneth L. Kelly,¹ Trenton T. Ross,¹ Kendra K. Bence,¹ and Min Wan¹

¹WRDM Internal Medicine Research Unit, Pfizer Inc, Cambridge, Massachusetts; ²WRDM Drug Safety, Research and Development, Pfizer Inc, Groton, Connecticut; ³WRDM Comparative Medicine, Pfizer Inc, Cambridge, Massachusetts; and ⁴WRDM Target Sciences, Pfizer Inc, Cambridge, Massachusetts



SUMMARY

Glycerol-3-phosphate acyltransferase 1 (GPAT1) deficiency in mice leads to consistent reduction of hepatic steatosis in obesity as well as in rodent NASH models. Interestingly, amelioration of liver inflammation and fibrosis was only observed when GPAT1-deficient mice were challenged with a choline-deficient, amino acid defined high-fat diet (CDAHFD).

BACKGROUND & AIMS: Nonalcoholic fatty liver disease (NAFLD), and its more severe form, nonalcoholic steatohepatitis (NASH), is the leading cause for liver failure and liver cancer. Although the etiology is likely multifactorial, genes involved in regulating lipid metabolism are enriched in human NAFLD genome-wide association studies (GWAS), pointing to dysregulated lipid metabolism as a major pathogenic factor. Glycerol-3-phosphate acyltransferase 1 (GPAT1), encoded by *GPAM*, converts acyl-CoAs and glycerol-3-phosphate into lysophosphatidic acid and has been shown

to regulate lipid accumulation in the liver. However, its role in mediating the progression from NAFLD to NASH has not been explored.

METHODS: GPAT1-deficient mice were generated and challenged with diets inducing hepatic steatosis and NASH. Effects of GPAT1 deficiency on lipid and systemic metabolic end points were evaluated.

RESULTS: Ablating GPAT1 globally or specifically in mouse hepatocytes reduced hepatic steatosis in the context of diet-induced or genetic obesity. Interestingly, blunting of progression from NAFLD to NASH in global GPAT1 knockout (KO) mice was model dependent. GPAT1 KO mice were protected from choline deficient, amino acid defined high-fat diet-induced NASH development, but not from the high fat, high carbohydrate, and high cholesterol diet-induced NASH.

CONCLUSIONS: Our preclinical data support the notion that lipid metabolism pathways regulated by GPAT1 in hepatocytes play an essential role in NASH progression, albeit in a model-dependent manner. (*Cell Mol Gastroenterol Hepatol* 2024; 17:279–291; <https://doi.org/10.1016/j.jcmgh.2023.10.002>)

Keywords: NASH; GPAT1; Hepatic Steatosis; Liver Inflammation and Fibrosis; NASH Mouse Models.

See editorial on page 311.

Nonalcoholic fatty liver disease (NAFLD) is characterized by excessive fat accumulation in the liver and has been estimated to affect as much as 25% of the population in the United States.¹ Approximately 20% of NAFLD patients progress to a more severe form of NAFLD, nonalcoholic steatohepatitis (NASH), which features hepatic steatosis, hepatocyte death, immune cell infiltration, and fibrosis.¹ Late-stage NASH may result in liver cirrhosis and liver cancer in humans.² NASH has become the leading cause of liver transplants and is an independent risk factor for type 2 diabetes and cardiovascular disease,^{3,4} which pose a huge medical burden globally. Unfortunately, there are currently no approved treatments for NASH, despite multiple classes of assets being evaluated in the clinic.⁵

Mechanisms that are associated with NAFLD and NASH etiology have been intensively studied in preclinical and clinical settings. Many fundamental questions remain unanswered, however, including identification of the critical driver(s) of NAFLD progression to NASH. Multiple anti-inflammatory and anti-fibrotic mechanisms have been deployed in the clinic to curb the progression of the disease; however, the outcome of these efforts to date has been largely disappointing.⁵ On the other hand, mechanisms targeting hepatic steatosis, such as thyroid hormone receptor β agonist Resmetirom, have generated promising results in the clinic (phase 3 MAESTRO-NASH trial, Madrigal Pharmaceuticals, Press Release, December 19, 2022). The notion that dysregulation of hepatic lipid metabolism drives NASH progression is well-supported by human genetics. The most impactful high-risk genes identified by genome-wide association studies (GWAS) to affect NASH-related traits in humans regulate lipid metabolism include *PNPLA3*, *TM6SF2*, *HSD17B13*, and *MBOAT7*.⁶ Recently, *GPAM* has been reported to be associated with circulating liver enzymes and chronic liver disease, adding to the existing list of lipid metabolism genes implicated in liver disease.^{6–11}

GPAM encodes glycerol-3-phosphate acyltransferase 1 (GPAT1) protein. GPAT1 is a member of the GPAT family of enzymes that convert glycerol-3-phosphate and acyl-CoAs into lysophosphatidic acid (LPA),¹² which is the first committed step of triglyceride and phospholipid synthesis. There are 4 members of the mammalian GPAT family. GPAT1 and GPAT2 localize on the outer membrane of mitochondria, whereas GPAT3 and GPAT4 are found on the endoplasmic reticulum.^{12,13} In hepatocytes, GPAT1 is the only mitochondrial GPAT and has been shown to account for about 50% of overall hepatic GPAT activity.¹⁴ Mice with GPAT1 deletion show reduced triglyceride (TG) synthesis and elevated fatty acid oxidation in the liver and are protected from diet-induced hepatic steatosis and insulin resistance.^{15,16} Meanwhile, overexpressing GPAT1 in the

liver leads to lipid accumulation and insulin resistance,^{17,18} which suggests a critical role of GPAT1 in modulating glucose and lipid metabolism. Consistently, knocking down or ablating GPAT1 in genetically obese (*ob/ob*) mice reduces liver fat content.^{19,20} Given the recent human GWAS findings associating *GPAM* with NASH,^{6–11} along with the evidence showing elevation of GPAT1 expression in preclinical NASH models,²¹ we hypothesized that GPAT1 could play an essential role in the pathogenesis of NAFLD progression to NASH. To address this hypothesis, we generated whole-body GPAT1 knockout (KO) mice and tested the impact on NAFLD and NASH phenotypes.

Results


Deletion of GPAT1 Protects Mice From Diet-Induced Hepatic Steatosis

To investigate GPAT1 function in modulating lipid metabolism, whole-body GPAT1 KO mice were generated using CRISPR-Cas9 technology. As expected, GPAT1 protein is absent in the liver of KO mice (Figure 1A), validating the KO model. Consistent with previous reports, GPAT1 KO mice are viable and fertile and have no obvious phenotypes.²²

To confirm its activity on regulating glucose and lipid metabolism, GPAT1 KO mice were challenged with a high-fat diet (HFD) for 10 weeks. Body weights were similar between wild-type (WT) and GPAT1 KO mice on HFD, with a slightly lower body weight observed in GPAT1 KO mice at week 9 of HFD feeding (Figure 1B). GPAT converts glycerol-3-phosphate and acyl-CoAs into LPA, and palmitoyl-CoA has been reported to be the preferred substrate for GPAT1.²³ Consistent with a lack of hepatic GPAT1 activity, a dramatic reduction of multiple LPA species was observed in GPAT1 KO mice compared with littermate controls, with 1-palmitoyl LPA (16:0-LPA) showing the most robust reduction (Figure 1C). Correspondingly, several species of liver acylcarnitines were elevated (Figure 1D), indicating the reshuffling of acyl-CoA into a more mitochondrial accessible pool in the liver of GPAT1 KO mice.¹⁵

Disrupting GPAT1 in mice significantly reduced liver TG content when subjected to HFD (Figure 1E). Lower circulating plasma TG and cholesterol were also observed in the GPAT1 KO mice, whereas alanine aminotransferase (ALT)

Abbreviations used in this paper: AAV, adeno-associated virus; ALT, alanine aminotransferase; AST, aspartate aminotransferase; BHBA, β -hydroxybutyrate; CDAHFD, choline deficient, amino acid defined high-fat diet; CFSE, carboxyfluorescein succinimidyl ester; EV, empty vector; GAN diet, high fat, high carbohydrate, and high cholesterol diet; GPAT1, glycerol-3-phosphate acyltransferase 1; GWAS, genome-wide association studies; HFD, high-fat diet; H/R ratio, hepatic to renal ratio; IL, interleukin; KO, knockout; LPA, lysophosphatidic acid; MRM, multiple reaction monitoring; NAFLD, nonalcoholic fatty liver disease; NASH, nonalcoholic steatohepatitis; NEFA, non-esterified fatty acids; PSR, picrosirius red; α -SMA, alpha-smooth muscle actin; SWE, shear wave elastography; TBG, human thyroxine binding globulin; TG, triglyceride; WT, wild-type.

 Most current article

© 2024 The Authors. Published by Elsevier Inc. on behalf of the AGA Institute. This is an open access article under the CC BY-NC-ND license (<http://creativecommons.org/licenses/by-nc-nd/4.0/>).

2352-345X

<https://doi.org/10.1016/j.jcmgh.2023.10.002>

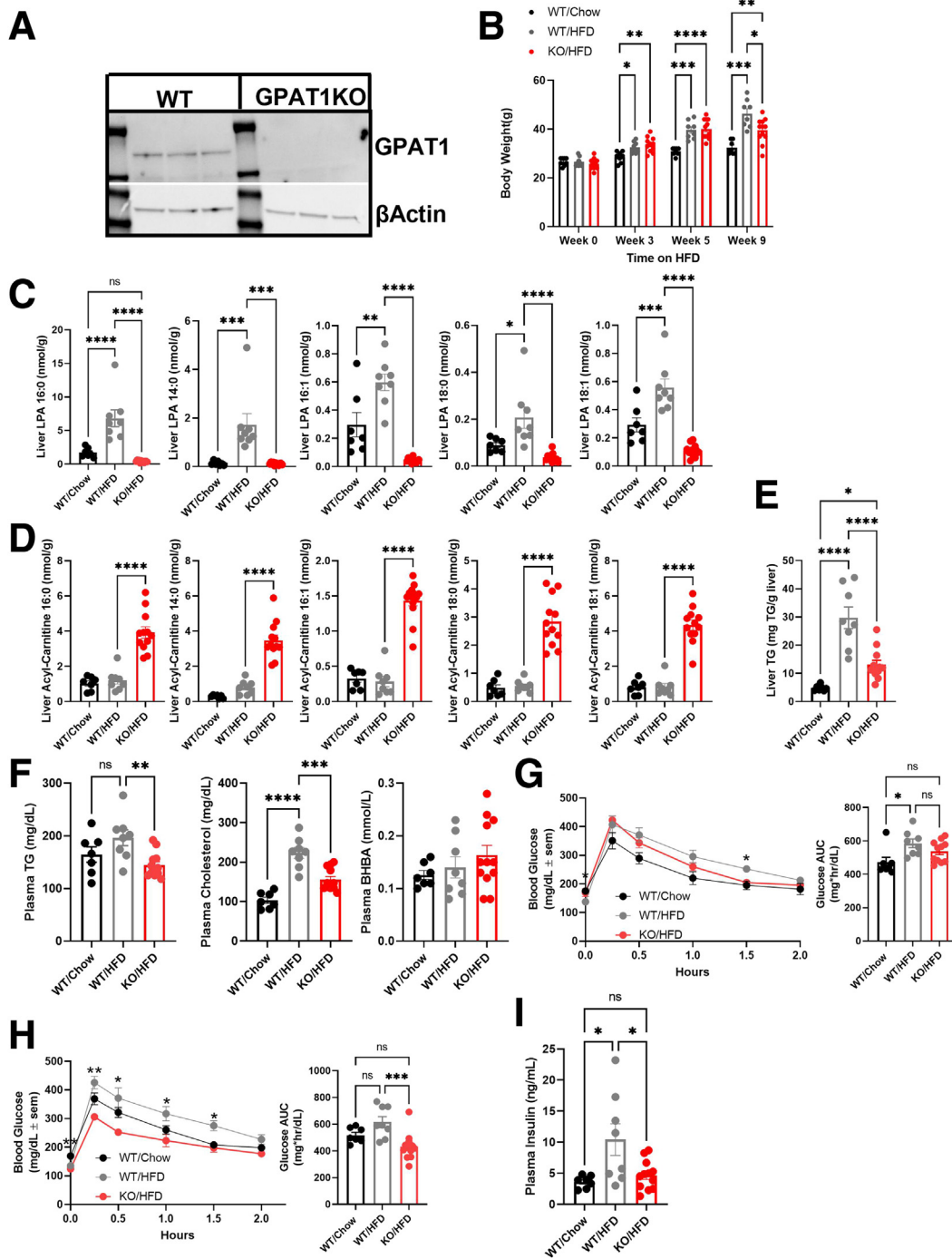


Figure 1. GPAT1 KO mice are protected from HFD-induced hepatic steatosis and glucose intolerance. (A) Western blot of WT and GPAT1 KO livers of mice fed with HFD for 10 weeks to confirm genotype. (B) Body weight of animals after 10 weeks on diet. (C) Quantification of liver LPA content. (D) Quantification of liver acylcarnitine species. (E) Liver TG content. (F) Plasma TG, cholesterol, and BHBA levels. (G) Glucose tolerance test (GTT) curves in WT and GPAT1-KO mice after 3 weeks of diet. Bars to the right show area under the curve (AUC) quantification of blood glucose monitoring during GTT. (H) GTT curves of WT and GPAT1-KO mice after 9 weeks of diet. Bars to the right represent AUC quantification during the GTT. (I) Fed plasma insulin after 10 weeks on HFD. Data represent mean \pm standard error of the mean. Samples represent biological replicates. Statistical analysis was performed by one-way analysis of variance with Tukey correction.

and aspartate aminotransferase (AST) levels were normal, and β -hydroxybutyrate (BHBA) levels were similar to WT controls (Figure 1F). GPAT1 KO mice also displayed slightly improved glucose tolerance after 3-week and 9-week HFD

feeding (Figure 1G and H) and blunted HFD-induced elevation of fed plasma insulin (Figure 1I). Taken together, these data are consistent with GPAT1 as a critical contributor to total liver metabolic flux and demonstrate a role for

GPAT1 in HFD-induced hepatic steatosis and glucose tolerance in mice.

Because GPAT1 is a minor contributor to overall GPAT activity in extrahepatic tissues, it is unlikely that extrahepatic GPAT1 drives liver fat reduction, although this possibility cannot be excluded considering GPAT1 is also expressed in adipose tissue. GPAT3 is the predominant adipose tissue GPAT isoform and accounts for ~80% of overall GPAT activity.²⁴ Mice with GPAT3 ablation gain less fat mass, but there is no change in liver fat content when fed HFD,²⁴ suggesting that GPAT activity in adipose tissue is dispensable for hepatic steatosis. To assess whether GPAT1 modulates obesity-induced hepatic steatosis in a hepatocyte autonomous manner, we generated *Gpam*^{lox/lox} mice using CRISPR-Cas9 technology and bred them with genetically obese, leptin-deficient *ob/ob* mice. To delete GPAT1 specifically in hepatocytes, *ob/ob; Gpam*^{lox/lox} mice were injected intravenously with adeno-associated virus (AAV) carrying an empty vector (EV) or a CRE-recombinase driven by a human thyroxine binding globulin (TBG) promoter.

No body weight changes were observed in the hepatocyte specific GPAT1 KO mice regardless of their obesity background (Figure 2A). In mice injected with AAV-TBG-CRE, levels of hepatic LPA species were reduced (Figure 2B), demonstrating a major disruption of hepatic GPAT1 flux. Elevation of acylcarnitines was also observed in the liver of the AAV-TBG-Cre injected mice, consistent with what we observed in the whole-body GPAT1 KO mice (Figure 2C).

Similar to the whole-body GPAT1 KO mice, a reduction in liver TG content was observed in the *ob/ob; Gpam*^{lox/lox} mice when injected with AAV-TBG-Cre compared with AAV-EV controls (Figure 2D), supporting the notion that GPAT1 deficiency protects against liver fat accumulation in a hepatocyte autonomous manner. Plasma BHBA levels were increased in hepatic GPAT1 KO mice (Figure 2E), suggesting a shuffling of acyl-CoAs for oxidation in the hepatocytes.¹⁵ However, the differences disappeared when bred into the *ob/ob* background, likely because of higher ketone levels in the *ob/ob* mice (Figure 2E). No major changes in plasma TG or non-esterified fatty acids (NEFA) were observed in these mice (Figure 2E). Notably, there were lower circulating ALT and AST levels in the hepatocyte-specific GPAT1 KO mice (Figure 2F), suggesting that obesity-induced liver injury is reduced. Overall, these data provide convincing evidence to show that loss of GPAT1 is protective for obesity-induced hepatic steatosis and liver injury in a hepatocyte autonomous manner.

GPAT1 Deletion Prevents Choline Deficient, Amino Acid Defined High-Fat Diet-Induced NASH Progression

Ameliorating hepatic steatosis is an attractive strategy for treating NASH in humans.¹ Because GPAT1 ablation consistently reduces liver fat content in mice, we investigated whether deletion of GPAT1 prevents NASH development.

Choline deficient, amino acid defined high-fat diet (CDAHFD) has been shown to rapidly promote NASH development in mice.²⁵ To assess whether GPAT1

modulates NASH phenotypes, GPAT1 KO mice and littermate controls were subjected to CDAHFD feeding for 12 weeks. As shown in previous experiments, GPAT1 deletion led to significant reduction of hepatic 16:0-LPA (Figure 3A). The levels of several LPA species were lower and acylcarnitines were higher in the liver of GPAT1 KO mice (Figure 3A and B). GPAT1 KO mice displayed no significant body weight differences compared with their littermate controls over the course of the experiment (Figure 3C). A noninvasive imaging tool, shear wave elastography (SWE), was used to monitor the progression of liver fat accumulation and predict liver fibrosis in mice. The hepatic to renal ratio (H/R ratio) is a diagnostic parameter that correlates with hepatic steatosis.²⁶ A significant increase in H/R ratio was seen in the control mice as early as 3 weeks on CDAHFD compared with chow-fed mice and persisted throughout the study. This increase in H/R ratio was blunted by GPAT1 deficiency at all time points measured in the study (Figure 3D), demonstrating that knocking out GPAT1 protected mice from CDAHFD-induced hepatic steatosis. At the end of the 12-week study, liver fat content was about 50% lower in the GPAT1 KO mice fed on CDAHFD compared with littermate controls, validating the observations from the noninvasive imaging study (Figure 3E). Histologic analysis on the liver samples also confirmed the reduction in steatosis in GPAT1 KO mice (Figure 3F). Plasma TG levels were lower in GPAT1 KO mice than in WT control mice when fed on chow diet, but no differences were observed when fed with CDAHFD (Figure 3G). CDAHFD feeding decreased plasma cholesterol and increased plasma BHBA levels in WT mice, and knocking out GPAT1 restored plasma cholesterol levels (Figure 3G). These data suggest that the regulation of lipid profile by GPAT1 could be heavily influenced by diet composition in mice.

Encouraged by the prevention of hepatic steatosis in GPAT1 KO mice on CDAHFD, we evaluated the impact on NASH progression. Similar to the *ob/ob* model, CDAHFD-induced elevation of plasma ALT and AST was moderately reduced in the GPAT1 KO mice (Figure 4A), suggesting a protective effect of GPAT1 deletion against the progression of liver injury in this NASH model. Furthermore, the expression of inflammatory (*Ccl2*, *Il-1 β* , *Il6*, *TNF α* , and *Ifny*) and fibrosis markers (*Acta2*, *Col1a1*, *Timp1*, and *Tgfb β 1*) was induced in WT mice fed on CDAHFD but was significantly lower in the liver of GPAT1 KO mice (Figure 4B and C). Consistently, the expected increase in SWE stiffness in WT littermate controls over the course of the study was almost completely blocked in the GPAT1 KO mice (Figure 4D), indicating that deletion of GPAT1 markedly slowed the progression to liver fibrosis. CDAHFD feeding increased hepatic Iba1 staining, a pan-macrophage marker, in control mice, suggesting enhancement of macrophage infiltration and induction of liver inflammation (Figure 4E). Significantly reduced Iba1 staining was seen in the liver of GPAT1 KO mice, consistent with attenuated liver inflammation (Figure 4E). Picrosirius red (PSR) staining is often used to detect collagen deposition in tissues, and alpha-smooth muscle actin (α -SMA) is a myofibroblast marker to quantify activated hepatic stellate cells, which is a major

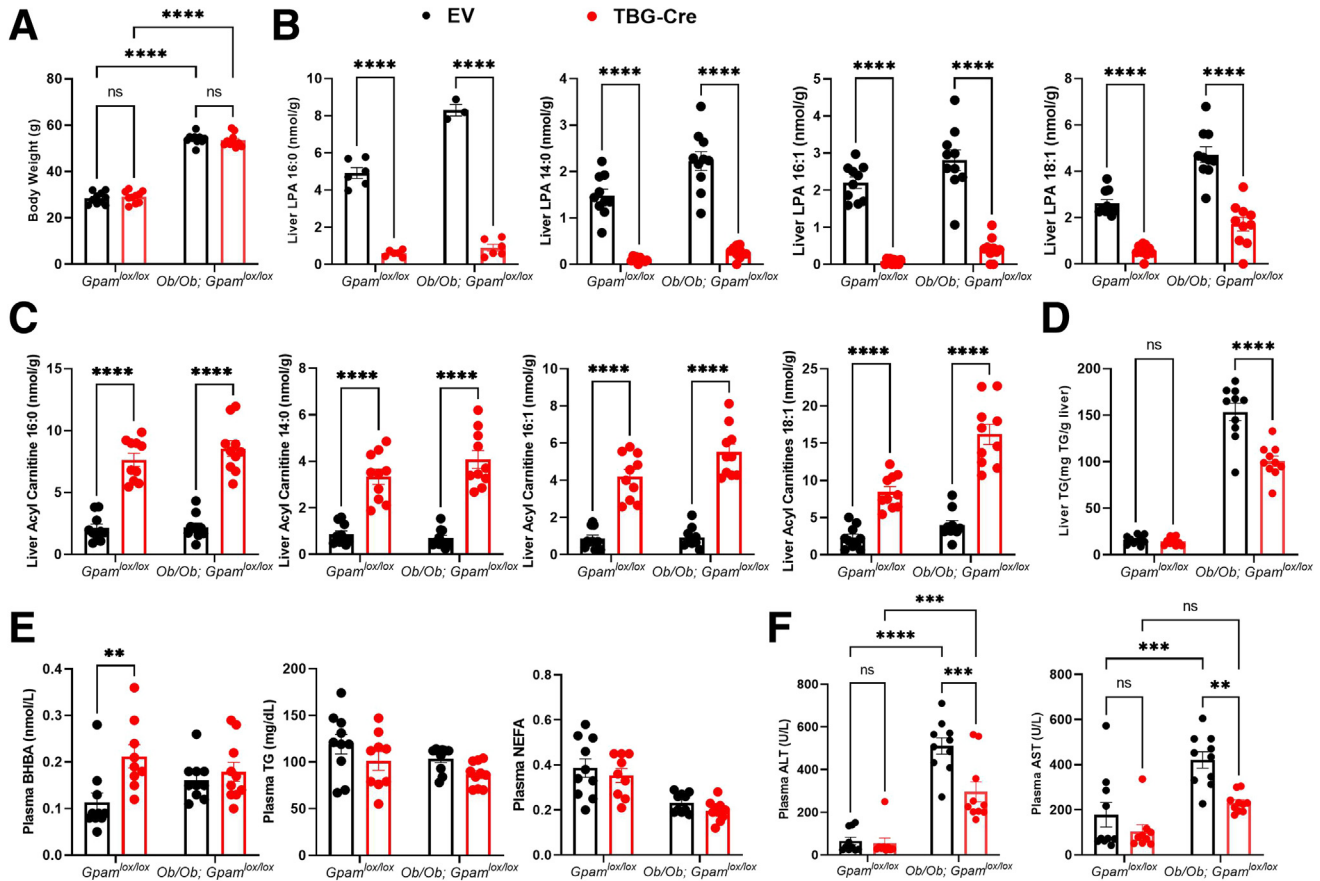


Figure 2. Deletion of GPAT1 specifically in hepatocytes reduced liver TG accumulation in *ob/ob* mice. (A) Body weight of *GPAT1^{lox/lox}* mice or *ob/ob; GPAT1^{lox/lox}* mice injected with either AAV-EV or AAV-TBG-CRE and left on chow for 4 weeks ($n = 10$ for each group). (B) Liver LPA content. (C) Liver acylcarnitine levels. (D) Liver TG content. (E) Plasma BHBA, TG, and NEFA levels. (F) Plasma ALT and AST levels. Data represent mean \pm standard error of the mean. Samples represent biological replicates. Statistical analysis was performed by two-way analysis of variance with Sidak correction.

contributor of collagen production and drives liver fibrosis.²⁷ Twelve-week CDAHFD feeding strongly increased PSR and α -SMA staining in the littermate control mice (Figure 4F and G); however, in the GPAT1 KO mice, hepatic PSR staining and α -SMA staining were dramatically reduced (Figure 4F and G). In conclusion, these data demonstrate that GPAT1 deletion in mice dramatically reduces hepatic steatosis, inflammation, and fibrosis induced by CDAHFD.

GPAT1 KO Mice Are Protected From High Fat, High Carbohydrate, and High Cholesterol Diet-Induced Hepatic Steatosis, But Not From Liver Inflammation and Fibrosis

Given the promising findings in the CDAHFD model, the effects of GPAT1 deficiency were evaluated in another commonly used preclinical NASH model, the high fat, high carbohydrate, and high cholesterol diet model (GAN).²⁸ Mice fed with the GAN diet for 24 weeks develop robust hepatic steatosis and display mild liver inflammation and fibrosis with elevated liver enzymes, recapitulating phenotypic characteristics of human NASH.²⁸ GPAT1 KO mice were

subjected to GAN diet feeding for 24 weeks, and the impact on NASH progression was assessed.

Consistent with previous observations, GPAT1 KO mice on GAN diet displayed significantly reduced levels of liver LPA and elevated acylcarnitine content (Figure 5A and B), confirming disruption of hepatic GPAT1 activity. No body weight differences were observed between WT and GPAT1 KO mice on GAN diet (Figure 5C). At the end of the 24-week study, $\sim 50\%$ reduction of liver TG content was observed in the GPAT1 KO mice (Figure 5D). Plasma TG levels were lower in GPAT1 KO mice only when the mice were fed with chow, but not on GAN diet (Figure 5E). GAN diet treatment increased plasma cholesterol levels and ketone levels significantly in WT mice; however, only the increase of cholesterol levels was blunted in GPAT1 KO mice (Figure 5E). Once again, these data showed that the regulation of lipid metabolism by GPAT1 is compounded by the dietary composition in mice. H/R ratio clearly showed an induction of hepatic steatosis in WT littermate controls as early as week 7 and persisting to week 19 (Figure 5F). Unlike the CDAHFD study, however, GPAT1 deficiency in mice did not change the H/R ratio on the GAN diet (Figure 5F), even though histologic analysis on the liver

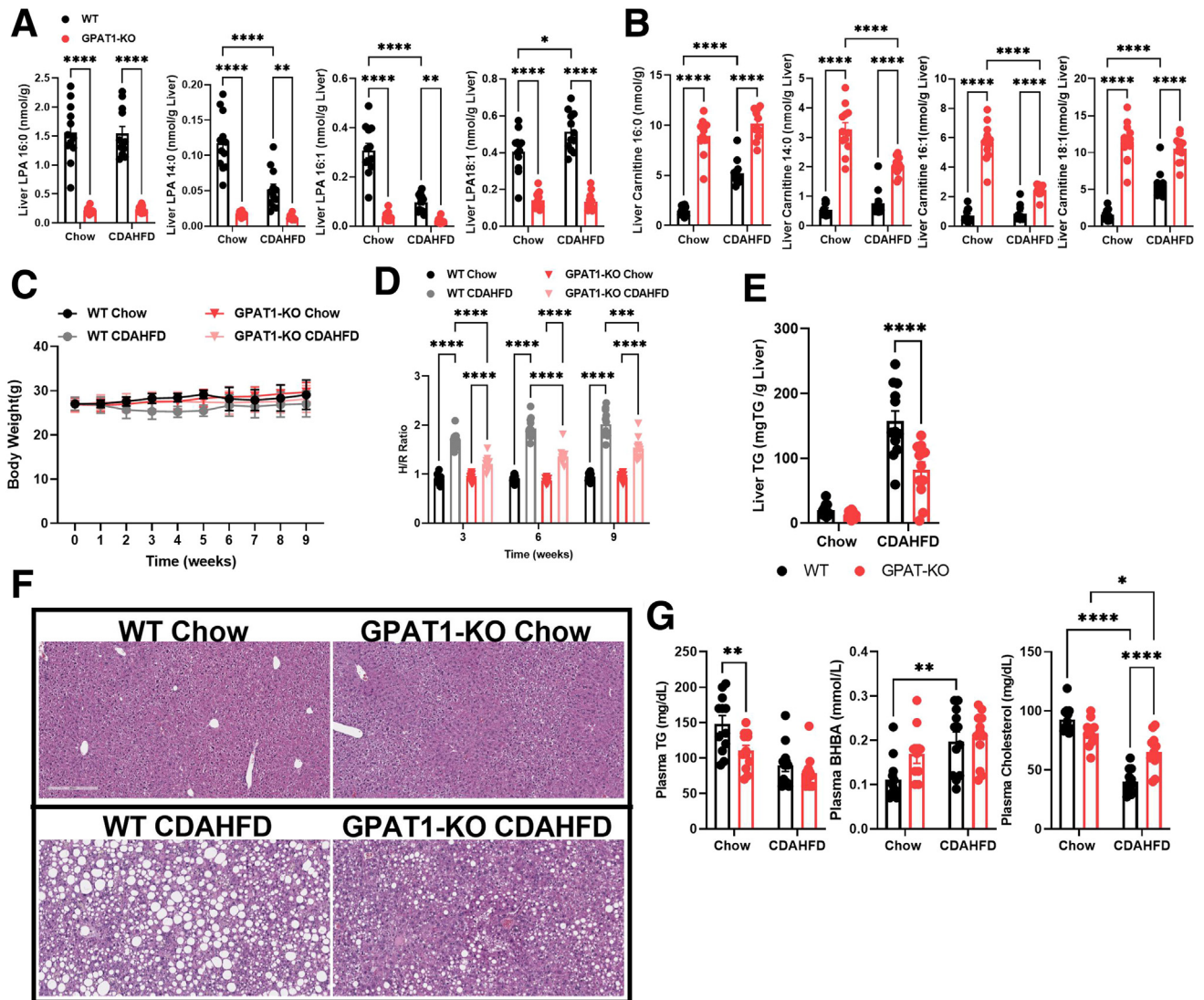


Figure 3. GPAT1 KO mice are protected from CDAHFD-induced liver steatosis. (A) Quantification of liver LPA content after 12 weeks of CDAHFD feeding. (B) Quantification of liver acylcarnitine species. (C) Body weight curves of WT and GPAT1-KO mice for duration of the diet study ($n = 12$ for each group). (D) H/R ratio from SWE for liver steatosis in WT and GPAT1-KO mice over the course of CDAHFD feeding. (E) Liver TG content. (F) Representative images of hematoxylin-eosin staining of liver sections from WT and GPAT1-KO mice after 12 weeks of diet. (G) Measurement of plasma analytes after 10 weeks of diet. Data represent mean \pm standard deviation of the mean. Samples represent biological replicates. Statistical analysis was performed by two-way analysis of variance with Sidak correction.

samples confirmed the reduction in steatosis in GPAT1 KO mice (Figure 5G). It is unclear why H/R ratio measured by imaging did not detect changes; however, we cannot exclude the possibility that the reduction of liver TG in GPAT1 KO mice measured at 24 weeks on diet is prominent only after week 19 when the last H/R ratio was measured.

The 24-week GAN diet feeding robustly increased plasma ALT and AST levels in WT control mice; however, GPAT1 deletion did not affect the induction in liver enzymes (Figure 6A). Hepatic expression of *Ccl2* and *TNF α* was significantly induced by GAN diet in both WT and GPAT1 KO mice; however, *IL-1 β* , *IL6*, and *IFN γ* expression in the liver was unchanged in response to GAN diet (Figure 6B). The fibrosis genes *Col1a1*, *Timp1*, and *TGF β* were induced to a

similar extent by GAN diet in both WT and GPAT1 KO mice, whereas *Acta2* expression was not altered (Figure 6C). Unlike the CDAHFD model, SWE recorded little progression of liver stiffness in WT and GPAT1 KO mice on GAN diet (Figure 6D). Further histologic analyses were performed to assess liver inflammation and fibrosis in this model. Liver inflammation and fibrosis were trending higher in the WT mice after 24-week GAN diet feeding, as shown by Iba1 and PSR staining, and this increase was slightly more robust in the GPAT1 KO mice (Figure 6E and F), although the differences between WT and KO mice on GAN diet were not statistically significant. These data showed that despite reducing hepatic steatosis, deleting GPAT1 did not prevent liver inflammation and fibrosis induced by GAN diet feeding.

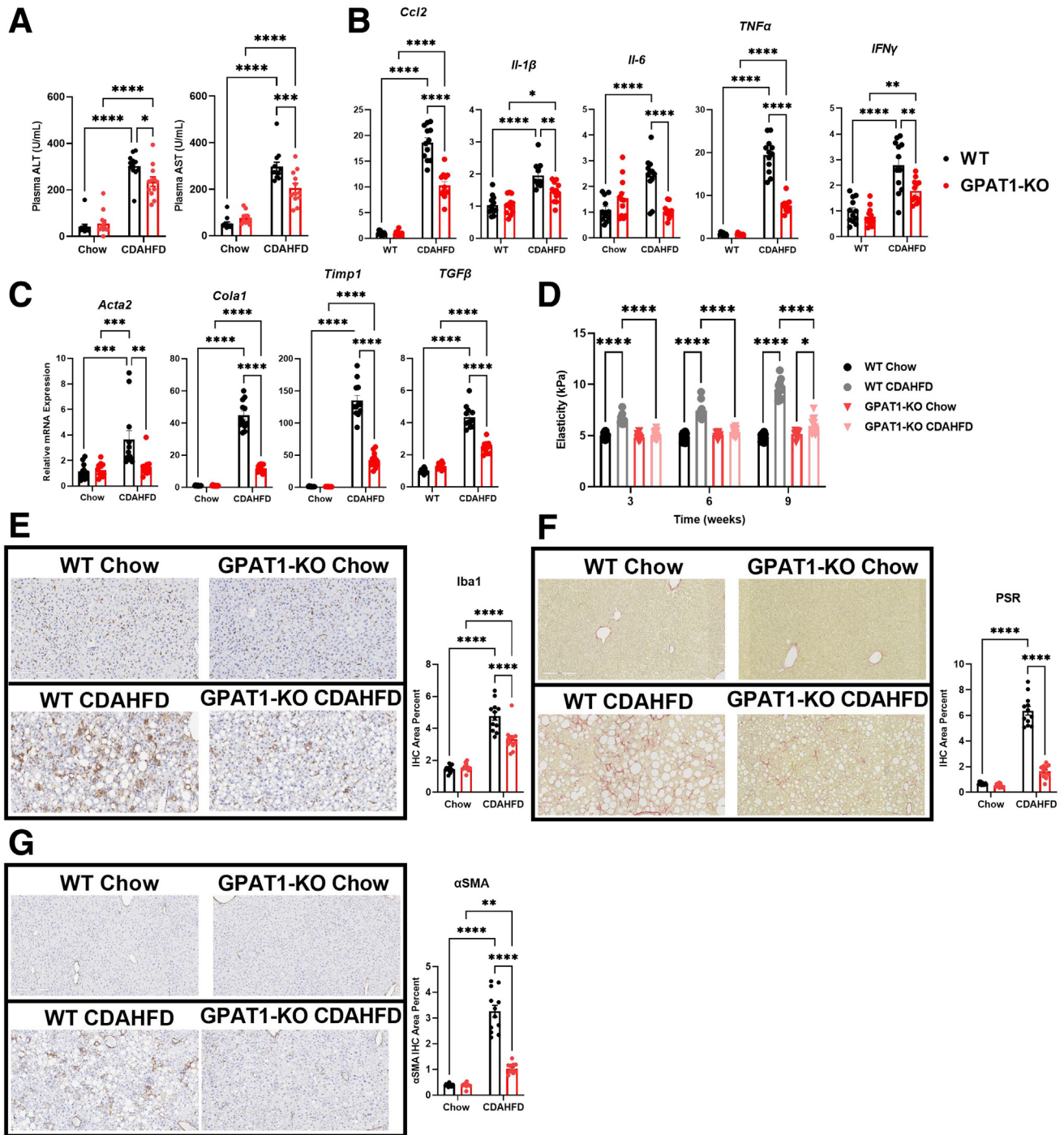


Figure 4. GPAT1 KO mice are resistant to liver inflammation and fibrosis induced by CDAHFD. (A) Plasma ALT and AST of WT and GPAT1-KO mice after 12 weeks of CDAHFD feeding. (B) Representative inflammatory gene expression panel in WT and GPAT1-KO livers. (C) Representative fibrotic gene expression panel in WT and GPAT1-KO livers. (D) SWE of livers to measure liver stiffness over the course of CDAHFD feeding. (E) Representative images of Iba1 immunohistochemical staining of fixed livers. *Bar graph* to the right represents positive Iba1 area in WT and GPAT1-KO livers. (F) Representative images of PSR staining of fixed livers. *Bar graph* to the right represents positive PSR area in WT and GPAT1-KO livers. (G) Representative images of α -SMA staining of fixed livers. *Bar graph* to the right represents positive α -SMA area in WT and GPAT1-KO livers. Data represent mean \pm standard error of the mean. Samples represent biological replicates. Statistical analysis was performed by two-way analysis of variance with Sidak correction.

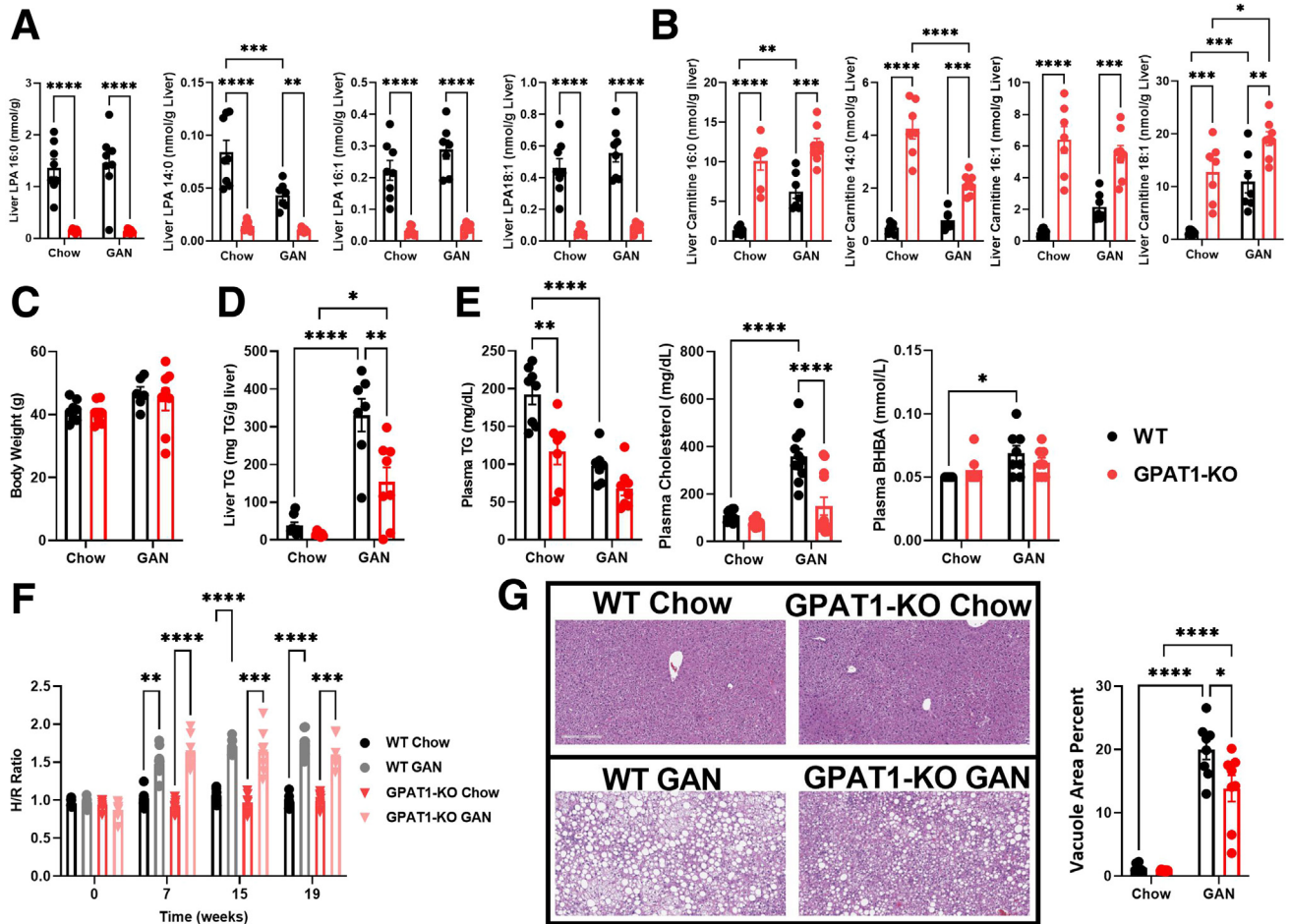


Figure 5. Reduced liver TG accumulation is observed in GPAT1 KO mice fed with GAN diet. (A) Liver LPA content in WT and GPAT1-KO mice fed GAN diet for 24 weeks ($n = 7-8$ for each group). (B) Liver acylcarnitine species content in WT and GPAT1-KO mice. (C) Body weight of WT and GPAT1-KO mice. (D) Liver TG content. (E) Plasma TG, cholesterol, and BHBA levels. (F) H/R ratio from SWE for liver steatosis in WT and GPAT1-KO mice over the course of GAN feeding. (G) Representative images of hematoxylin-eosin staining of liver sections from WT and GPAT1-KO mice after 24 weeks of diet. Bar graph to the right represents vacuole area percent of liver. Data represent mean \pm standard error of the mean. Samples represent biological replicates. Statistical analysis was performed by two-way analysis of variance with Sidak correction.

One potential difference between the GAN and CDAHFD models could be related to the role of GPAT1 in immune cells. CDAHFD incites a robust immune cell infiltration and activation in the liver, subsequently resulting in strong liver fibrosis (Figure 4E–G). However, mice fed with GAN diet only showed subtle elevation of liver inflammation and fibrosis (Figure 6E and F). These data imply that the efficiency of protecting against NASH progression in these models could be sensitive to the robustness of a certain mechanism that would affect immune cell function. GPAT1 deletion has been previously reported to reduce T-cell proliferation and Th1 cytokine release in mice.²⁹ To see whether proliferation of T cells is affected with GPAT1 deletion, naive CD4⁺ T cells were isolated from the spleen of male and female WT and GPAT1 KO mice and stimulated with CD3/CD28 antibodies. CD4⁺ T cells isolated from GPAT1 KO female mice showed defective proliferation compared with female WT controls measured by carboxyfluorescein succinimidyl ester (CFSE) staining;

however, no proliferation defect was observed in CD4⁺ T cells isolated from male GPAT1 KO mice (Figure 7A). Similarly, upon CD3/CD28 stimulation, production of interleukin (IL) 2, IL 4, IL 10, and interferon gamma from GPAT1 KO CD4⁺ T cells isolated from female mice was significantly dampened, and only IL 2 secretion caught up with the WT cells at the 48-hour time point; however, little differences were observed in male CD4⁺ T cells between genotypes (Figure 7B). Interestingly, the production of tumor necrosis factor alpha was reduced by around 50% in male CD4⁺ T cells isolated from GPAT1 KO male mice (Figure 7B); however, it is uncertain how much that could contribute to reduced inflammation and fibrosis because the major source of tumor necrosis factor alpha in the liver is monocytes/macrophages.³⁰ Because all NASH diet experiments were run with male mice in our studies, it is unlikely that the model-dependent outcomes can be explained by T-cell activity of GPAT1 KO mice, even though we cannot exclude the possibility that functions of

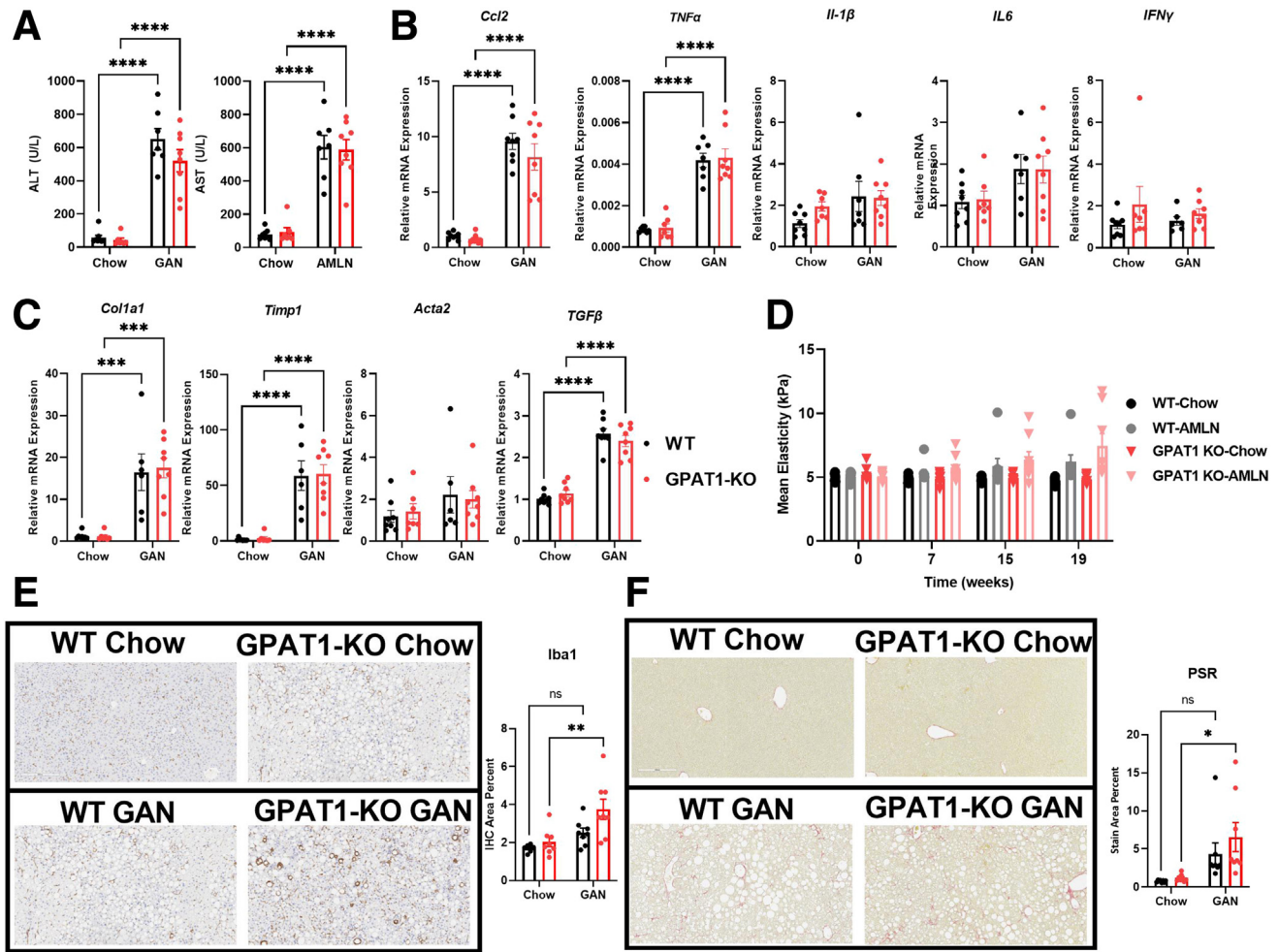


Figure 6. Liver inflammation and fibrosis are not affected in GPAT1 KO mice when challenged with GAN diet. (A) Plasma ALT and AST of WT and GPAT1-KO mice after 24 weeks of GAN feeding ($n = 7-8$ for each group). (B) Representative inflammatory gene expression panel in WT and GPAT1-KO livers. (C) Representative fibrotic gene expression panel in WT and GPAT1-KO livers. (D) SWE of livers to measure liver stiffness over the course of GAN diet feeding. (E) Representative images of Iba1 immunohistochemical staining of fixed livers. Bar graph below represents positive Iba1 area in WT and GPAT1-KO livers. (F) Representative images of PSR staining of fixed livers. Bar graph below represents positive PSR area in WT and GPAT1-KO livers. Data represent mean \pm standard error of the mean. Samples represent biological replicates. Statistical analysis was performed by two-way analysis of variance with Sidak correction.

GPAT1 in other types of immune cells may play a role in various aspects of NASH progression.

Discussion

NAFLD/NASH is becoming the leading cause of liver failure and liver cancer and is an independent risk factor for metabolic syndrome like type 2 diabetes and cardiovascular diseases in humans.^{1,3,4} Even though the etiology of NASH remains unclear, multiple human GWAS have identified genes that are involved in lipid metabolism as causal for NAFLD/NASH progression, suggesting that dysregulated lipid metabolism is one of the culprits.⁶

GPAM, which encodes GPAT1 in humans, has recently been identified as a causal gene that associates with NAFLD and NASH.⁶⁻¹¹ GPAT1 catalyzes the conversion of glycerol-3-phosphate and acyl-CoA into LPA, which is the first

committed step for neutral lipid and phospholipid synthesis.¹⁴ In addition to its role in controlling lipid synthesis, GPAT1 has also been shown to affect very low-density lipoprotein associated TG secretion in the liver, presented by reduced circulating TG in GPAT1 KO mice.^{16,22,31,32} Lower plasma TG levels were indeed observed in GPAT1 KO mice compared with WT controls when fed on chow diet in our studies (Figure 1F). However, the differences disappeared when mice were treated with CDAHFD or GAN diet (Figures 3G and 5E), arguing against lipid secretion as the major mechanism for GPAT1 to regulate hepatic lipid metabolism. Interestingly, the association of GPAM with plasma TG in humans goes in the opposite direction of metabolic and NASH traits,^{8,9} indicating that blocking GPAT1 could lead to elevated TG in circulation.

GPAT1 has also been proposed to control the fate of acyl-CoAs for lipid synthesis versus oxidation in the liver.¹⁵

though the protection of liver inflammation and fibrosis by GPAT1 ablation in mice appears to be model dependent, the findings in human GWAS support the notion that GPAT1 plays a critical role in the progression of NAFLD and NASH.

Materials and Methods

All authors had access to the study data and reviewed and approved the final manuscript.

Animal Studies

All procedures performed on animals were in accordance with regulations and established guidelines and were reviewed and approved by an Institutional Animal Care and Use Committee or through an ethical review process. Whole-body GPAT1 KO male mice and their WT littermate counterparts were synthesized in house, and the colony was maintained at Charles River Laboratories (Wilmington, MA). At 8–12 weeks of age, animals were brought on-site and acclimated for 1 week in thermoneutral conditions before the beginning of the experiment. Animals were housed under standard laboratory conditions and kept on a 12:12 hour light-dark cycle. Four separate cohorts of mice were used to complete this study.

In the first cohort, mice were randomized into 3 groups based on age and body weight and then placed onto a chow (Teklad, 2920) or a coconut-oil based HFD (Research Diets, D12331) for 10 weeks. An oral glucose tolerance test was performed 3 weeks and 9 weeks after introduction to diet by fasting the mice for 6 hours before the start of the tolerance test and gavaging with 1 g glucose/kg body weight. Blood glucose levels were monitored for 2 hours after bolus by glucose monitor (AlphaTrak). After 10 weeks of diet, animals were euthanized, and tissues were collected for analysis.

For the second cohort of animals, we generated *GPAM^{lox/lox}* mice using CRISPR-Cas9 technology and bred these animals with the genetic obese strain deficient of *leptin* (*ob/ob* mice). To delete GPAT1 specifically in hepatocytes, *GPAM^{lox/lox}* mice were injected intravenously with AAV carrying a CRE-recombinase driven by a human TBG promoter. Eight-week-old *ob/ob*; *GPAM^{lox/lox}* mice were injected with either AAV-TBG-Cre or control AAV carrying an empty vector (AAV-EV) and followed for 8 weeks after injection.

For the GAN diet study, male WT and GPAT1 KO littermates, aged 8–12 weeks, were acclimated at thermoneutral conditions for 1 week before the start of the experiment. Animals were randomized by age and body weight before being placed onto chow or GAN diet (Research Diets, 09100310) for 32 weeks. Body weights were measured weekly. On weeks 7, 16, and 20, SWE was conducted, animals were fasted overnight, and 200 μ L of whole blood was taken by submandibular bleeding for future analysis.

In the final cohort of animals, mice were randomized into 4 groups based on age and body weight and then placed onto a chow (Teklad, 2920) or a choline-deficient high fat diet (Research Diets, A06071302i) for 12 weeks. Body weight was taken weekly, and every 3 weeks, SWE was conducted. SWE was performed using an Aixplorer Ultimate

system (SuperSonic Imagine, Aix-en-Provence, France) with a 6- to 2-MHz linear array (SuperLinear SLH20-6; SuperSonic Imagine) transducer. All animals were fasted for approximately 4–6 hours prior to minimize interference of gut contents and gut movement during image acquisition.

On the last day of the study, mice were euthanized by CO₂ asphyxiation for tissue collection, and blood was collected by cardiac puncture. Plasma samples were analyzed on a Siemens Chemistry XPT clinical analyzer. Livers were rapidly removed for histology, and the remaining were frozen in liquid N₂. Frozen livers were pulverized on a N₂ cooled aluminum block. Powdered liver was stored at –80°C for further analysis.

Histology

Livers were rapidly removed, and the right lateral, medial, and left lateral lobes were excised, and approximately 3-mm sections were placed into 10% neutral buffered formalin and processed to paraffin blocks using standard tissue processing protocols for histology. The staining procedures and protocols used have been previously described.²⁵

Hepatic Triglyceride Content

Powdered liver was weighed and homogenized using lysis tubes containing 500 μ L TG lysis buffer (140 mmol/L, 50 mmol/L Tris, pH 7.4, 0.1% Triton X-100). Samples were diluted in phosphate-buffered saline and vortexed. An equal amount of sample and sodium deoxycholate was added to a clear bottom 96-well plate, vortexed, and incubated at 37°C for 5 minutes. Two hundred μ L of Infinity Triglyceride Reagent (Thermo Fisher Scientific) was added to each sample, incubated at 37°C for 20 minutes, and read on the Spectramax5 spectrophotometer (Molecular Devices, San Jose, CA). TG content was normalized to liver weight.

Immunoblotting

Liver tissue samples were homogenized in RIPA buffer (50 mmol/L Tris-HCL, pH 8.0, 150 mmol/L NaCl, 1% NP-40, 0.5% w/v sodium deoxycholate, and 0.1% w/v sodium dodecyl sulfate) with 1 \times protease inhibitors and 1 \times protease/phosphatase inhibitors (Cell Signaling). Protein samples were subjected to sodium dodecyl sulfate-polyacrylamide gel electrophoresis using a 4%–12% bis-tris gradient gel (Bio-Rad) and transferred onto a nitrocellulose membrane. Membranes were incubated overnight against antibodies against GPAM (Novus Biologicals) and β -actin (Sigma), followed by fluorescently conjugated secondary antibodies (Licor) and detection on the Licor Odyssey. Immunoblot intensities were quantified using the Licor Image studio analysis software.

Gene Expression Analysis

Mouse livers were homogenized in Trizol (Invitrogen), and RNA was isolated using RNeasy Mini Kit (Qiagen) following the manufacturer's protocol. RNA was quantified using the Lunatic (Unchained Labs, Pleasanton, CA) and

converted to cDNA using Applied Biosystem's High-Capacity cDNA Reverse Transcription Kit (Thermo Fisher Scientific) following the manufacturer's protocol. Gene expression was measured using TaqMan Gene Expression Assay.

Liver LPA and Acylcarnitines Measurement and Analysis

LPA and acylcarnitines were extracted from liver tissue using an acidified Bligh-Dyer method. To 25 mg of frozen pulverized liver tissue was added 400 μ L methanol containing labeled acylcarnitine standards (Cambridge Isotopes NSK-B) and U-13C LPA 16:0 (Avanti Polar lipids 790661). Four hundred μ L of 0.1M HCl was added and vortexed to mix. Four hundred μ L of chloroform was then added and mixed. Samples were centrifuged at 5000 rpm for 8 minutes to facilitate phase separation. The organic layer was collected and dried under a stream of nitrogen. The residue was then resuspended in ethanol for liquid chromatography coupled to tandem mass spectrometry analysis. Liquid chromatography coupled to tandem mass spectrometry analysis was performed on a Shimadzu Nexera X2 LC system coupled to a Sciex 6500+ mass spectrometer. Sample separation was performed using a Millipore SeQuant ZIC-CHILIC 3 μ m, 100 \times 2.1 mm column. Mobile phase A was 100% acetonitrile, and mobile phase B was 50 mmol/L ammonium acetate in 50% methanol 50% water. The separation gradient began at 10% B at 0.2 mL/min for 5 minutes, then increased to 25% B over 2 minutes, and held for 7 minutes, followed by a 5-minute re-equilibration at 10% B. Scheduled multiple reaction monitorings (MRMs) were performed to accommodate polarity switching. Acylcarnitine detection was performed in positive mode from 4–6 minutes, and MRMs for each acylcarnitine species monitored the carnitine head group fragment at m/z 85. LPA detection was performed in negative mode from 9–12 minutes, and MRMs for each LPA species monitored the head group fragment at m/z 153. Quantitation was performed relative to the single point internal standard.

Statistical Analysis

All data were reported as the means \pm standard error of the mean. Intergroup treatment effects in the CDAHFD and GAN diet were assessed using 2-way analysis of variance, with the post hoc Sidak test for multiple comparisons. Statistical significance was set to 0.05. SWE data were analyzed using a mixed-effect model repeat measurement, with regimen, week, and regimen * week interaction as fixed factors and animal as a random factor. Least-squares means estimates, least-squares means differences between regimens at each time point, along with their respective 95% confidence interval and *P* values, were calculated. Statistical significance was set at .05. For histologic analysis, nonparametric statistics were used, and group values were reported as \pm semi-interquartile range. The Mann-Whitney test was used to compare the quantity of target in liver sections. Significance was set to 0.05.

References

1. Bence KK, Birnbaum MJ. Metabolic drivers of non-alcoholic fatty liver disease. *Mol Metab* 2021;50:101143.
2. Cholaneril G, Patel R, Khurana S, et al. Hepatocellular carcinoma in non-alcoholic steatohepatitis: current knowledge and implications for management. *World J Hepatol* 2017;9:533–543.
3. Goldberg D, Ditah IC, Saeian K, et al. Changes in the prevalence of hepatitis C virus infection, nonalcoholic steatohepatitis, and alcoholic liver disease among patients with cirrhosis or liver failure on the waitlist for liver transplantation. *Gastroenterology* 2017;152:1090–1099 e1.
4. Lonardo A, Nascimbeni F, Mantovani A, et al. Hypertension, diabetes, atherosclerosis and NASH: cause or consequence? *J Hepatol* 2018;68:335–352.
5. Aggarwal P, Nouredin M, Harrison S, et al. Nonalcoholic steatohepatitis (NASH) cirrhosis: a snapshot of therapeutic agents in clinical development and the optimal design for clinical trials. *Expert Opin Investig Drugs* 2022;31:163–172.
6. Du X, DeForest N, Majithia AR. Human genetics to identify therapeutic targets for NAFLD: challenges and opportunities. *Front Endocrinol (Lausanne)* 2021;12:777075.
7. Hakim A, Moll M, Brancale J, et al. Genetic variation in the mitochondrial glycerol-3-phosphate acyltransferase is associated with liver injury. *Hepatology* 2021;74:3394–3408.
8. Sveinbjornsson G, Ulfarsson MO, Thorolfsdottir RB, et al. Multiomics study of nonalcoholic fatty liver disease. *Nat Genet* 2022;54:1652–1663.
9. Chen Y, Du X, Kuppa A, et al. Genome-wide association meta-analysis identifies 17 loci associated with nonalcoholic fatty liver disease. *Nat Genet* 2023.
10. Jamialahmadi O, Mancina RM, Ciociola E, et al. Exome-wide association study on alanine aminotransferase identifies sequence variants in the GPAM and APOE associated with fatty liver disease. *Gastroenterology* 2021;160:1634–1646 e7.
11. Vujkovic M, Ramdas S, Lorenz KM, et al. A multiethnic genome-wide association study of unexplained chronic ALT elevation as a proxy for nonalcoholic fatty liver disease with histological and radiological validation. *Nat Genet* 2022;54:761–771.
12. Gonzalez-Baro MR, Coleman RA. Mitochondrial acyltransferases and glycerophospholipid metabolism. *Biochim Biophys Acta Mol Cell Biol Lipids* 2017;1862:49–55.
13. Johnson ZL, Ammirati M, Wasilko DJ, et al. Structural basis of the acyl-transfer mechanism of human GPAT1. *Nat Struct Mol Biol* 2023;30:22–30.
14. Coleman RA, Lee DP. Enzymes of triacylglycerol synthesis and their regulation. *Prog Lipid Res* 2004;43:134–176.
15. Hammond LE, Neschen S, Romanelli AJ, et al. Mitochondrial glycerol-3-phosphate acyltransferase-1 is essential in liver for the metabolism of excess acyl-CoAs. *J Biol Chem* 2005;280:25629–25636.

16. Neschen S, Morino K, Hammond LE, et al. Prevention of hepatic steatosis and hepatic insulin resistance in mitochondrial acyl-CoA:glycerol-sn-3-phosphate acyltransferase 1 knockout mice. *Cell Metab* 2005;2:55–65.
17. Linden D, William-Olsson L, Ahnmark A, et al. Liver-directed overexpression of mitochondrial glycerol-3-phosphate acyltransferase results in hepatic steatosis, increased triacylglycerol secretion and reduced fatty acid oxidation. *FASEB J* 2006;20:434–443.
18. Nagle CA, An J, Shiota M, et al. Hepatic overexpression of glycerol-sn-3-phosphate acyltransferase 1 in rats causes insulin resistance. *J Biol Chem* 2007;282:14807–14815.
19. Xu H, Wilcox D, Nguyen P, et al. Hepatic knockdown of mitochondrial GPAT1 in ob/ob mice improves metabolic profile. *Biochem Biophys Res Commun* 2006;349:439–448.
20. Wendel AA, Li LO, Li Y, et al. Glycerol-3-phosphate acyltransferase 1 deficiency in ob/ob mice diminishes hepatic steatosis but does not protect against insulin resistance or obesity. *Diabetes* 2010;59:1321–1329.
21. Liao K, Pellicano AJ, Jiang K, et al. Glycerol-3-phosphate acyltransferase1 is a model-agnostic node in nonalcoholic fatty liver disease: implications for drug development and precision medicine. *ACS Omega* 2020;5:18465–18471.
22. Hammond LE, Gallagher PA, Wang S, et al. Mitochondrial glycerol-3-phosphate acyltransferase-deficient mice have reduced weight and liver triacylglycerol content and altered glycerolipid fatty acid composition. *Mol Cell Biol* 2002;22:8204–8214.
23. Vancura A, Haldar D. Purification and characterization of glycerophosphate acyltransferase from rat liver mitochondria. *J Biol Chem* 1994;269:27209–27215.
24. Cao J, Perez S, Goodwin B, et al. Mice deleted for GPAT3 have reduced GPAT activity in white adipose tissue and altered energy and cholesterol homeostasis in diet-induced obesity. *Am J Physiol Endocrinol Metab* 2014;306:E1176–E1187.
25. Ross TT, Crowley C, Kelly KL, et al. Acetyl-CoA carboxylase inhibition improves multiple dimensions of NASH pathogenesis in model systems. *Cell Mol Gastroenterol Hepatol* 2020;10:829–851.
26. Morin J, Swanson TA, Rinaldi A, et al. Application of ultrasound and shear wave elastography imaging in a rat model of NAFLD/NASH. *J Vis Exp* 2021.
27. Venturi C, Reding R, Quinones JA, et al. Relevance of activated hepatic stellate cells in predicting the development of pediatric liver allograft fibrosis. *Liver Transpl* 2016;22:822–829.
28. Hansen HH, HM AE, Oro D, et al. Human translatability of the GAN diet-induced obese mouse model of non-alcoholic steatohepatitis. *BMC Gastroenterol* 2020;20:210.
29. Collison LW, Murphy EJ, Jolly CA. Glycerol-3-phosphate acyltransferase-1 regulates murine T-lymphocyte proliferation and cytokine production. *Am J Physiol Cell Physiol* 2008;295:C1543–C1549.
30. Parameswaran N, Patial S. Tumor necrosis factor-alpha signaling in macrophages. *Crit Rev Eukaryot Gene Expr* 2010;20:87–103.
31. Kim CW, Addy C, Kusunoki J, et al. Acetyl CoA carboxylase inhibition reduces hepatic steatosis but elevates plasma triglycerides in mice and humans: a bedside to bench investigation. *Cell Metab* 2017;26:576.
32. Lewin TM, de Jong H, Schwerbrock NJ, et al. Mice deficient in mitochondrial glycerol-3-phosphate acyltransferase-1 have diminished myocardial triacylglycerol accumulation during lipogenic diet and altered phospholipid fatty acid composition. *Biochim Biophys Acta* 2008;1781:352–358.
33. Richardson TG, Leyden GM, Wang Q, et al. Characterising metabolomic signatures of lipid-modifying therapies through drug target mendelian randomisation. *PLoS Biol* 2022;20:e3001547.
34. Kano K, Aoki J, Hla T. Lysophospholipid mediators in health and disease. *Annu Rev Pathol* 2022;17:459–483.
35. Baader M, Bretschneider T, Broermann A, et al. Characterization of the properties of a selective, orally bioavailable autotaxin inhibitor in preclinical models of advanced stages of liver fibrosis. *Br J Pharmacol* 2018;175:693–707.
36. Irifune H, Kochi Y, Miyamoto T, et al. GPAM mediated lysophosphatidic acid synthesis regulates mitochondrial dynamics in acute myeloid leukemia. *Cancer Sci* 2023.

Received August 21, 2023. Accepted October 11, 2023.

Correspondence

Address correspondence to: Min Wan, PhD, WRDM Internal Medicine Research Unit, Pfizer Inc1 Portland Street, Cambridge, Massachusetts 02139. e-mail: Min.Wan@pfizer.com.

Acknowledgments

The authors thank Drs Xin Rong and Gregory Tesz for scientific discussions. They thank Sripad Ram, Andrew Robbertson, Elizabeth Rebhun, Gary Seitis, Sarah Vargas, and Alan Opsahl (WRDM Drug Safety, Research and Development, Pfizer Inc) for helping preparation of the histology samples and image analyses. They thank Jennifer Zhang, Anna Yeh, and Allison Brill for their contribution to the research.

CRedit Authorship Contributions

Min Wan (Conceptualization: Lead; Supervision: Lead; Writing – original draft: Lead; Writing – review & editing: Lead)
 Kathleen R. Smith (Conceptualization: Supporting; Data curation: Lead; Writing – original draft: Supporting; Writing – review & editing: Supporting)
 Wenshan Wang (Conceptualization: Supporting; Data curation: Supporting)
 Melissa R. Miller (Data curation: Supporting; Formal analysis: Supporting; Writing – original draft: Supporting)
 Magalie Boucher (Data curation: Supporting; Formal analysis: Supporting; Writing – original draft: Supporting; Writing – review & editing: Supporting)
 Jessica Reynold (Data curation: Supporting; Formal analysis: Supporting)
 Natalie A. Daurio (Data curation: Supporting; Formal analysis: Supporting)
 Dongmei Li (Data curation: Supporting; Formal analysis: Supporting)
 Dinesh Hirehallur-Shanthappa (Data curation: Supporting; Formal analysis: Supporting)
 Youngwook Ahn (Data curation: Supporting; Formal analysis: Supporting)
 David Beebe (Data curation: Supporting; Formal analysis: Supporting)
 Kenneth Kelly (Data curation: Supporting; Formal analysis: Supporting)
 Trenton Ross (Conceptualization: Supporting; Data curation: Supporting; Formal analysis: Supporting)
 Kendra Bence (Conceptualization: Equal; Writing – original draft: Supporting; Writing – review & editing: Supporting)

Conflicts of interest

All authors are current or former employees of Pfizer, Inc and may be shareholders of Pfizer, Inc.

Funding

The study presented herein was funded by Pfizer, New York, New York.